AGU PUBLICATIONS

Global Biogeochemical Cycles

RESEARCH ARTICLE
10.1002/2014GB005048

Water mass age and aging driving chromophoric dissolved organic matter in the dark global ocean

T. S. Catalá[1], I. Reche[1], M. Álvarez[2], S. Khatiwala[3], E. F. Guallart[4], V. M. Benítez-Barrios[5], A. Fuentes-Lema[6], C. Romera-Castillo[4,7], M. Nieto-Cid[7], C. Pelejero[4,8], E. Fraile-Nuez[5], E. Ortega-Retuerta[4], C. Marrasé[4], and X. A. Álvarez-Salgado[7]

[1]Departamento de Ecología and Instituto del Agua, Universidad de Granada, Granada, Spain, [2]IEO Centro Oceanográfico de A Coruña, Coruña, Spain, [3]Department of Earth Sciences, University of Oxford, Oxford, UK, [4]CSIC Institut de Ciències del Mar, Barcelona, Spain, [5]IEO Centro Oceanográfico de Canarias, Santa Cruz de Tenerife, Spain, [6]Departamento de Ecoloxía e Bioloxía Animal, Universidade de Vigo, Vigo, Spain, [7]CSIC Instituto de Investigacións Mariñas, Vigo, Spain, [8]Institució Catalana de Recerca i Estudis Avançats, Barcelona, Spain

Key Points:
- First global census of CDOM variables of the main water masses of the ocean
- Effect of "age" and "aging" on CDOM optical properties
- Turnover time of CDOM in the dark global ocean

Supporting Information:
- Figures S1 and S2
- Table S1

Correspondence to:
T. S. Catalá,
teresascatala@gmail.com

Citation:
Catalá, T. S., et al. (2015), Water mass age and aging driving chromophoric dissolved organic matter in the dark global ocean, *Global Biogeochem. Cycles*, *29*, 917–934, doi:10.1002/2014GB005048.

Received 4 DEC 2014
Accepted 30 MAY 2015
Accepted article online 2 JUN 2015
Published online 7 JUL 2015

Abstract The omnipresence of chromophoric dissolved organic matter (CDOM) in the open ocean enables its use as a tracer for biochemical processes throughout the global overturning circulation. We made an inventory of CDOM optical properties, ideal water age (τ), and apparent oxygen utilization (AOU) along the Atlantic, Indian, and Pacific Ocean waters sampled during the Malaspina 2010 expedition. A water mass analysis was applied to obtain intrinsic, hereinafter archetypal, values of τ, AOU, oxygen utilization rate (OUR), and CDOM absorption coefficients, spectral slopes and quantum yield for each one of the 22 water types intercepted during this circumnavigation. Archetypal values of AOU and OUR have been used to trace the differential influence of water mass aging and aging rates, respectively, on CDOM variables. Whereas the absorption coefficient at 325 nm (a_{325}) and the fluorescence quantum yield at 340 nm (Φ_{340}) increased, the spectral slope over the wavelength range 275–295 nm ($S_{275-295}$) and the ratio of spectral slopes over the ranges 275–295 nm and 350–400 nm (S_R) decreased significantly with water mass aging (AOU). Combination of the slope of the linear regression between archetypal AOU and a_{325} with the estimated global OUR allowed us to obtain a CDOM turnover time of 634 ± 120 years, which exceeds the flushing time of the dark ocean (>200 m) by 46%. This positive relationship supports the assumption of in situ production and accumulation of CDOM as a by-product of microbial metabolism as water masses turn older. Furthermore, our data evidence that global-scale CDOM quantity (a_{325}) is more dependent on aging (AOU), whereas CDOM quality ($S_{275-295}$, S_R, Φ_{340}) is more dependent on aging rate (OUR).

1. Introduction

The pool of oceanic dissolved organic matter (DOM) represents, besides soil humus, the largest reservoir of organic matter of the biosphere [*Hedges*, 1992]. It contains around 700 Pg of carbon, which is equivalent to that of CO_2 in the atmosphere (750 Pg) [*Siegenthaler and Sarmiento*, 1993; *Hansell*, 2013]. Most marine organic matter is originated from phytoplankton photosynthesis in the surface ocean; the vast majority (80%) of the organic matter that enters the ocean interior is particulate organic matter (POM), either suspended or sinking, and the dissolved fraction (DOM) represents 20% of total organic carbon flux [*Carlson et al*., 1994; *Six and Maier-Reimer*, 1996; *Hansell et al*., 2009] and serves as substrate supporting heterotrophic prokaryotic metabolism [*Hansell*, 2013]. At present, the global carbon flux to the ocean interior as DOM is about 2 Pg C yr^{-1} [*Hansell et al*., 2009; *Hansell*, 2013], which is similar to the annual ocean uptake of anthropogenic CO_2 [*Gruber et al*., 2009].

Most of the phytoplankton-derived organic matter is biologically labile and has a very short lifetime (hours to days), being quickly respired back to CO_2 in the illuminated zone. However, a portion of the fixed carbon that escapes rapid mineralization is transformed (biotically or abiotically) into resistant material and accumulates as recalcitrant DOM (RDOM), creating the enormous ocean reservoir of dissolved organic carbon (DOC) [*Hansell et al*., 2009, 2012; *Hansell*, 2013]. The microbial-mediated transformation of labile into refractory DOM was first postulated by *Ogawa et al*. [2001] and was termed as "microbial carbon pump" (MCP) by *Jiao et al*. [2010], who formalized the idea in a wider context. *Benner and Herndl* [2011] estimated that approximately 23% of the bulk oceanic DOC pool (155 Pg C) was sequestered by the MCP in the global

ocean and *Kattner et al*. [2011] and *Arrieta et al*. [2015] suggested the low concentration of the thousands of individual DOM constituents in the deep ocean as a possible cause for the inability of prokaryotes to use RDOM as a carbon source. In this study, we provide new insights to the RDOM characterization and its distribution by taking advantage of the ability of a fraction of the RDOM to absorb light.

The fraction of dissolved organic matter (DOM) that absorbs light in the ultraviolet and, to a lesser extent, in the visible range of the spectrum is named chromophoric dissolved organic matter (CDOM). Typically, UV-visible absorption spectra for CDOM increase exponentially with decreasing wavelength [*Twardowski et al*., 2004]. To obtain information about the origin, processing, and fate of CDOM from the spectra, several variables have been described and can be gathered into (1) "Quantitative" variables (i.e., absorption coefficients at specific wavelengths), which are a proxy of the CDOM concentration (being 254 and 325 nm the most commonly used wavelengths) and (2) "Qualitative" variables (i.e., spectral slopes, molar extinction coefficients, absorption coefficient ratios, and quantum yields), which are largely independent of the concentration and provide information about the origin, molecular weight, and chemical structure of CDOM [*Brown*, 1977; *Weishaar et al*., 2003; *Helms et al*., 2008; *Nelson and Siegel*, 2013].

The first attempts to map the CDOM in the surface ocean were conducted to cope with the accuracy of global satellite-based measurements of ocean chlorophyll and primary production [*Siegel et al*., 2005; *Ortega-Retuerta et al*., 2010]. Since the interest on CDOM distribution throughout the water column is more recent, global databases are not still very abundant. Furthermore, most studies addressed this matter from a geographical perspective, describing differences among ocean basins and depths in epipelagic, mesopelagic, and bathypelagic layers [*Nelson et al*., 2007, 2010]. The novelty of our approach is that we describe the distribution of CDOM by considering the main water masses crossed by the circumnavigation. The aims of this study are (1) to make an inventory of the CDOM optical properties of the main water masses of the dark global ocean by using "quantitative" (i.e., absorption coefficients) and "qualitative" spectral variables, (2) to trace the basin-scale mineralization processes affecting these CDOM optical properties using a water mass analysis, (3) to estimate the turnover time of the CDOM in the dark ocean, and (4) to assess the effect of "age" and "aging" on CDOM optical properties. In this context, age is defined as the elapsed time since the water was last in contact with the atmosphere, and aging (traced through apparent oxygen utilization, AOU) refers to the consumption of oxygen over that period. To pursue our goals, we performed the following activities: (1) a water mass analysis to obtain the proportion of the main water types (WT) intercepted during the Malaspina 2010 circumnavigation in the central, intermediate, and abyssal waters of the global ocean; (2) an inventory of ideal ages, AOU, oxygen utilization rates (OUR), and spectral variables of the main water masses of the dark ocean; and (3) a regression analyses of the relationship of these spectral variables with the ideal age and aging (AOU) of the water masses at the global scale.

2. Materials and Methods

2.1. Sampling Site and Measurements

The Malaspina 2010 circumnavigation was conducted from December 2010 to July 2011 on board R/V *Hesperides* along the Atlantic, Indian, and Pacific Oceans, spanning latitudes from 34°N to 40°S (Figure 1). During the cruise, 147 conductivity-temperature-depth (CTD) stations were carried out with a Seabird 911+ from surface to 4000 m depth. Water samples were collected at each station with a 24–10 L Niskin bottles rosette. The CTD was equipped with a redundant temperature and salinity sensor for intercomparison during the cruise and a polarographic membrane oxygen sensor Seabird SBE-43. Temperature and pressure sensors were calibrated at the SeaBird laboratory before the cruise. Onboard salinity calibration was carried out with a Guildline AUTOSAL model 8410 A salinometer with a precision higher than 0.002 for single samples and the potentiometric end-point Winkler method for the calibration of the oxygen sensor. Oxygen saturation was calculated from practical salinity and potential temperature with the equation of *Benson and Krauss* [1984]. Apparent oxygen utilization (AOU) was calculated as the difference between the saturation and measured dissolved oxygen concentrations.

The UV-visible absorption coefficient of CDOM was determined from 250 to 750 nm at 1 nm intervals in 10 cm path length quartz cuvettes in a double-beam Perkin Elmer lambda 850 spectrophotometer. The estimated detection limit of this spectrophotometer for quantifying CDOM absorption is 0.001 absorbance units or 0.02 m^{-1}.

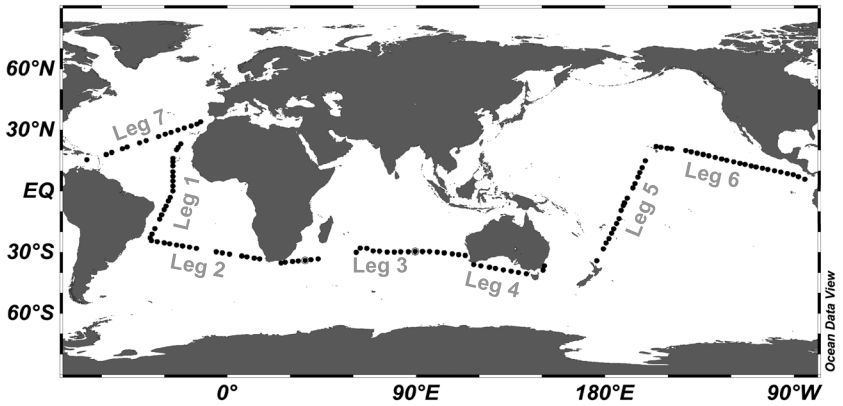

Figure 1. Cruise track of the Malaspina 2010 circumnavigation on board the Spanish R/V *Hespérides* from 16 December 2010 to 11 July 2011.

Samples for the determination of the absorption spectrum of CDOM were not filtered because light absorption due to pigments and detrital particles contribute only to a minor fraction of the open ocean CDOM absorption [*Nelson et al*., 1998, 2007], particularly at the depths (200–4000 m) covered by this study. At each station, samples were drawn from Niskin bottles at eight discrete depths throughout the water column, poured directly into acid cleaned 250 mL glass bottles and immediately stored in dark conditions to allow equilibration with room temperature and to avoid photobleaching. The time elapsed between sample collection and determination did not exceed 2 h. A blank was measured every five samples to detect and correct (linearly) any instrument drift. To minimize any effect of light scattering by particles and microbubbles, samples were stirred vigorously and then settled to let any particles fall to the bottom of the flask before measuring. During the measurements, we first checked that the differences between sample and baseline absorbance at long wavelengths (>600 nm) maintained <0.0005 absorbance units. In the case that difference was >0.0005 absorbance units, we renewed the water in the sample cuvette and repeated the measurement. In most cases, we got a final difference <0.0005 absorbance units. To correct this generally minor effect of light scattering, we applied a wavelength-independent correction proposed by *Green and Blough* [1994], which consists on subtracting the average absorbance in the 600–750 nm wavelength range to the measured absorption spectrum. We chose the wavelength-independent correction instead of the wavelength-dependent correction proposed by *Bricaud et al*. [1981] because the low differences between sample and baseline absorbance at long wavelengths did not produce measurable differences between both corrections at short wavelengths.

Absorbance at 325 nm was converted into absorption coefficient (m^{-1}, a_{325}) [*Green and Blough*, 1994] using the equation:

$$a_{325} = 2.303 \frac{[Abs_{325} - Abs_{600-750}]}{l} \quad (1)$$

where Abs_{325} is the absorbance at a wavelength of 325 nm, $Abs_{600-750}$ is the average absorbance between 600 and 750 nm, l is the path length of the cuvette (0.1 m), and 2.303 is the factor that converts from decadic to natural logarithms.

Helms et al. [2008] emphasized the potential of the spectral slopes as a tool for the structural characterization of CDOM and calculated them from the linear regression of log-transformed absorption spectra. They chose the 275–295 nm and 350–400 nm wavelength ranges because these are the intervals identified as the most dynamic regions of the natural log-transformed absorption spectra [*Helms et al*., 2013] and appear to be particularly sensitive to shifts in molecular weight or DOM sources [*Helms et al*., 2008]. After a previous quality check, those slopes with $R^2 < 0.95$ for $S_{275-295}$ and $R^2 < 0.85$ for $S_{350-400}$ were deleted. As a consequence, the data set of $S_{275-295}$ and $S_{350-400}$ were reduced from 742 to 737 and 717 samples, respectively. A dimensionless variable, the slope ratio (S_R), was calculated as the ratio of the slope of the shorter wavelength region (275–295 nm) to that of the longer wavelength region (350–400 nm).

The quantum yield of DOM fluorescence at excitation 340 nm, Φ_{340}, is the proportion of light absorbed at 340 nm, a_{340}, that is reemitted as fluorescent light between 360 and 560 nm, $F_{360-560}$, and was calculated as in *Green and Blough* [1994]:

$$\Phi_{340} = \Phi_{340(QS)} \frac{F_{360-560}}{a_{340}} \frac{a_{340(QS)}}{F_{360-560(QS)}} \quad (2)$$

where $\Phi_{340(QS)}$ is the dimensionless fluorescence quantum yield of quinine sulfate (the standard used to calibrate fluorescence measurements), 0.54 [*Melhuish*, 1961], and $F_{360-560}$ is the integral of fluorescence intensity at an excitation/emission of 340/360–560 nm. Fluorescence measurements were taken with a JY-Horiba Spex Fluoromax-4 spectrofluorometer and the sample scan was reported at an emission interval between 360 and 560 nm after exciting it at 340 nm. Fluorescence units were converted to Raman units dividing by the Raman area for further comparison with other studies (see more details in *Catalá et al*. [2015]). Whereas simple chemical structures containing carbon double bounds are capable of absorbing radiation, fluorescence emission is uniquely produced under the presence of the more complex aromatic rings. Therefore, higher values of Φ_{340} are indicative of a higher proportion of aromatic compounds [*Green and Blough*, 1994; *Romera-Castillo et al*., 2011].

2.2. Estimation of the Water Sample Age

Water sample ages (τ) were derived from *Khatiwala et al*. [2009, 2012] by interpolating their gridded mean age estimates to our sample time, locations, and depths. As described by these authors, they used an inverse technique to estimate the ocean's mean age from tracer observations. A mathematically rigorous approach that accounts for the multiplicity of transport pathways and transit times characteristic of an eddy-diffusive flow such as the ocean allowed them to quantify ventilation in terms of a probability distribution that partitions fluid parcels according to the time and location of their last contact with the surface. Such a distribution is known as a boundary propagator (or more generically a Green function). The ideal mean age is the first moment of the boundary propagator integrated over the entire surface of the ocean (sometimes called a "transit time distribution" or TTD) and is interpreted as the average time since a water parcel was last in contact with the surface. *Khatiwala et al*. [2009, 2012] developed a maximum entropy-based inverse technique to deconvolve the ocean's boundary propagator from tracer observations, which they applied to gridded fields of radiocarbon, cluorofluorocarbons (CFCs) and hydrographic (temperature, salinity, phosphate, and oxygen) data.

2.3. Water Mass Analysis

The dark ocean (from 200 m to the bottom) can be described by the mixing of distinct water masses. A water mass is a body of water defined by its intrinsic thermohaline and chemical characteristics that, in turn, can be described by one or more water types (WT) [*Tomczak*, 1999].

The strategy to sample the dark ocean during the Malaspina circumnavigation was not in favor of collecting water from fixed depth levels but from extreme values of salinity, temperature, and dissolved oxygen. This procedure allowed us covering the cores of flow of the most abundant WT of the dark global ocean (depth $\geq$ 200 m, $\theta < 18$°C, AOU > 0) and, therefore, performing a robust calculation of the different WT proportions that contribute to any of the 742 CDOM samples collected during the circumnavigation by means of a classical water mass analysis [*Karstensen and Tomczak*, 1998]. We have characterized the WT on basis of its salinity (S) and potential temperature (θ), which are assumed to be conservative variables.

The equations to be solved for a specific water sample j are

$$100 = \sum_i x_{ij} \quad (3)$$

$$\theta_j = \sum_i x_{ij} \cdot \theta_i \quad (4)$$

$$S_j = \sum_i x_{ij} \cdot S_i \quad (5)$$

where x_{ij} is the proportion of WT i in sample j; θ_j and S_j are the thermohaline characteristics of sample j; and θ_i and S_i are the fixed thermohaline characteristic of WT i in the area where it is defined. Furthermore, the solution of the multiparameter water mass analysis includes an additional constrain: all contributions must sum up to 100% and have to be nonnegative.

We have identified 22 water types in the route followed during the Malaspina 2010 circumnavigation [*Catalá et al.*, 2015] (Table S1 in the supporting information). They were divided into three domains according to their depth: central (200–500 m), intermediate (500–1500 m), and abyssal (>1500 m). In the central domain, we identified Eighteen Degrees Water (EDW), Eastern North Atlantic Central Water (ENACW), defined by two WT of 12°C and 15°C, 13°C water of the equatorial Atlantic (13EqAtl), South Atlantic Central Water (SACW), defined by two WT of 12°C and 18°C, Indian Subtropical Mode Water ($STMW_I$), Indian Central Water of 13°C (ICW_{13}), South Pacific Subtropical Mode Water ($STMW_{SP}$), South Pacific Central Water of 20°C ($SPCW_{20}$), 13°C water of the equatorial Pacific (13EqPac), North Pacific Subtropical Mode Water ($STMW_{NP}$), and North Pacific Central Mode Water (CMW_{NP}). In the intermediate domain we found Mediterranean Water (MW), Antarctic Intermediate Water (AAIW), defined by two WT of 3.1°C and 5.0°C, Sub-Antarctic Mode Water (SAMW) and North Pacific Intermediate Water (NPIW). In the abyssal domain we identified Circumpolar Deep Water (CDW), North Atlantic Deep Water (NADW), defined by two types of 2°C and 4.6°C, and Antarctic Bottom Water (AABW).

Equations (3)–(5) allow solving the simultaneous mixing of a maximum of three WT on basis of reasonable vertical and geographical constraints to the water mass mixing. Concerning the vertical constraints, for a given region of the ocean, every WT will mix only with the water types situated immediately above and below according to their density. Regarding the geographical constraints, every WT will mix preferentially with water types in their surroundings. With these considerations in mind, we deconvolved the 742 samples collected during the circumnavigation into 24 pairs/triads that group water samples with common WT composition (see Figure S1 in the supporting information).

2.4. Volume of Each Water Type Collected During the Malaspina Circumnavigation

Once the WT proportions (x_{ij}) are known, the fraction of the total volume of water sampled during the Malaspina 2010 circumnavigation that corresponds to WT i (%VOL_i) can be calculated as

$$\%VOL_i = \frac{\sum_j x_{ij}}{n} \tag{6}$$

where n is the number of samples.

2.5. Archetypal Values and OUR Estimation

The archetypal value of variable N for water type i (N_i) is the weighted-average value of N in the center of mass of WT_i in the study area. According to *Álvarez-Salgado et al.* [2013], archetypes retain information about the variability of N that can be attributed to mixing of water types and basin-scale mineralization processes from the site where the water types were defined to their respective centers of mass along the circumnavigation. Archetypal values of depth (z), water age (τ), apparent oxygen utilization (AOU), a_{325}, $S_{275-295}$, S_R and Φ_{340} were calculated for the 22 WT intercepted by the Malaspina cruise track as follows:

$$N_i = \frac{\sum_j x_{ij} \cdot N_j}{\sum_j x_{ij}} \tag{7}$$

where N_j is the value of variable N (z, τ, AOU, OUR, a_{325}, $S_{275-295}$, S_R, and Φ_{340}) in sample j and x_{ij} is the proportion of WT_i in sample j.

The standard deviation of N_i (SDN_i), which should be interpreted as an estimate of the robustness of the calculation, was obtained as

$$SDN_i = \frac{\sqrt{\sum_j x_{ij} \cdot (N_j - N_i)^2}}{\sum_j x_{ij}} \tag{8}$$

Similarly, the archetypal value of N in every sample ($<N_j>$) was calculated as

$$<N_j> = \frac{\sum_i x_{ij} \cdot N_i}{100} \tag{9}$$

The determination coefficient (R^2) and standard deviation of the residuals (SD res) of the linear regressions between the measured (N_j) and arquetypal values ($<N_j>$) of variable N were obtained. Whereas R^2 allows

assessing the degree of dependence of variable N on WT mixing and basin-scale mineralization in the dark ocean, SD res informs on the average error incurred when estimating the measured from the archetypal values.

Division of AOU_i (in $\mu mol\,kg^{-1}$) by τ_i (in years) provides a measure of the archetypal oxygen utilization rate (OUR) of each water type, an indicator of the velocity at which the mineralization of organic matter occurs in oxygenic environments [*Jenkins*, 1982]. Specifically, the archetypal oxygen utilization rate of each WT, OUR_i (in $\mu mol\,kg^{-1}\,yr^{-1}$), represents the average rate of oxygen consumption from the area where the WT_i is formed to its center of mass along the Malaspina cruise track. To perform this calculation, we have assumed that water masses are in equilibrium with the atmosphere in their formation areas (i.e., the initial AOU of any WT is 0). Since we are aware that this assumption may not be totally accurate [*Ito et al*., 2004], the OUR_i values obtained with this procedure could be, to some extent, overestimated.

2.6. Calculation of the Global Production of CDOM and Its Turnover Time

To estimate the CDOM production in the dark global ocean (see the results in section 3.4), we have followed the procedures applied by *Yamashita and Tanoue* [2008] and *Catalá et al*. [2015] to calculate the global production of marine fluorescent humic-like substances on the basis of the slope of the relationship between fluorescent dissolved organic matter (FDOM) and AOU but applied in our case to CDOM and AOU. Therefore, the global net production of a_{325}, NP_{a325} (in $m^{-1}\,yr^{-1}$), was obtained as

$$NP_{a325} = \left(\frac{\partial a_{325}}{\partial AOU}\right) \cdot OUR_{global} \tag{10}$$

where $\frac{\partial a_{325}}{\partial AOU}$ is the absorption coefficient rate of change per AOU unit for the global dark ocean and OUR_{global} is the total oxygen consumption rate that is obtained as

$$OUR_{global} = \frac{\sum_i VOL_i \cdot OUR_i}{100} \tag{11}$$

Once the NP_{a325} was obtained, we calculated the CDOM turnover time as [*Catalá et al*., 2015]

$$\text{Turnover time} = \frac{\sum_i VOL_i \cdot a_{325i}}{100 \cdot NP_{a325}} \tag{12}$$

where $\frac{\sum_i VOL_i \cdot a_{325i}}{100}$ is the WT proportion weighted-average a_{325} of the dark global ocean.

2.7. Statistical Analysis

Linear regression analyses between the different values (measured, archetypal) of τ, AOU, OUR, a_{325}, $S_{275-295}$, S_R and Φ_{340}, were performed using the Statistica 7.0 software. Linear regression analyses were also used for the Arrhenius plot (see section 3.2). We applied model II regressions because we have no control of the variables used [*Sokal and Rohlf*, 1995].

3. Results

3.1. WT Distribution in the Three Ocean Basins

A classical water mass analysis of the thermohaline properties of the central, intermediate, and abyssal waters (200–4000 m) of the North and South Atlantic, South Indian, and South and North Pacific Oceans was used to determine (i) the water mass proportions on each individual sample collected during the circumnavigation, (ii) the water mass proportion-weighted-average value of the different CDOM variables, and (iii) the variability of CDOM due to water mass mixing and basin-scale mineralization processes from the source point to the center of mass of the WT within the circumnavigation.

In this study, 22 WT were identified (Table S1 in the supporting information). We intercepted 13 central WT representing 26.3% of the total water volume sampled, with the 13EqPac accounting for 5.7% and spreading on the South and North Pacific at an archetypal depth (Z_i) of 483 ± 35 m (Figure 2a). We sampled five intermediate waters, representing 21.5% of the total volume, and the most prominent were SAMW, corresponding to 8.0% of the total volume and located mostly in the Indian Ocean and the Great Australian Bight at an archetypal depth (Z_i) of 719 ± 42 m (Figure 2b), AAIW, which accounted for 7.4% including its two branches (3.1 and 5.0°C) and was basically located in the South Atlantic and below the

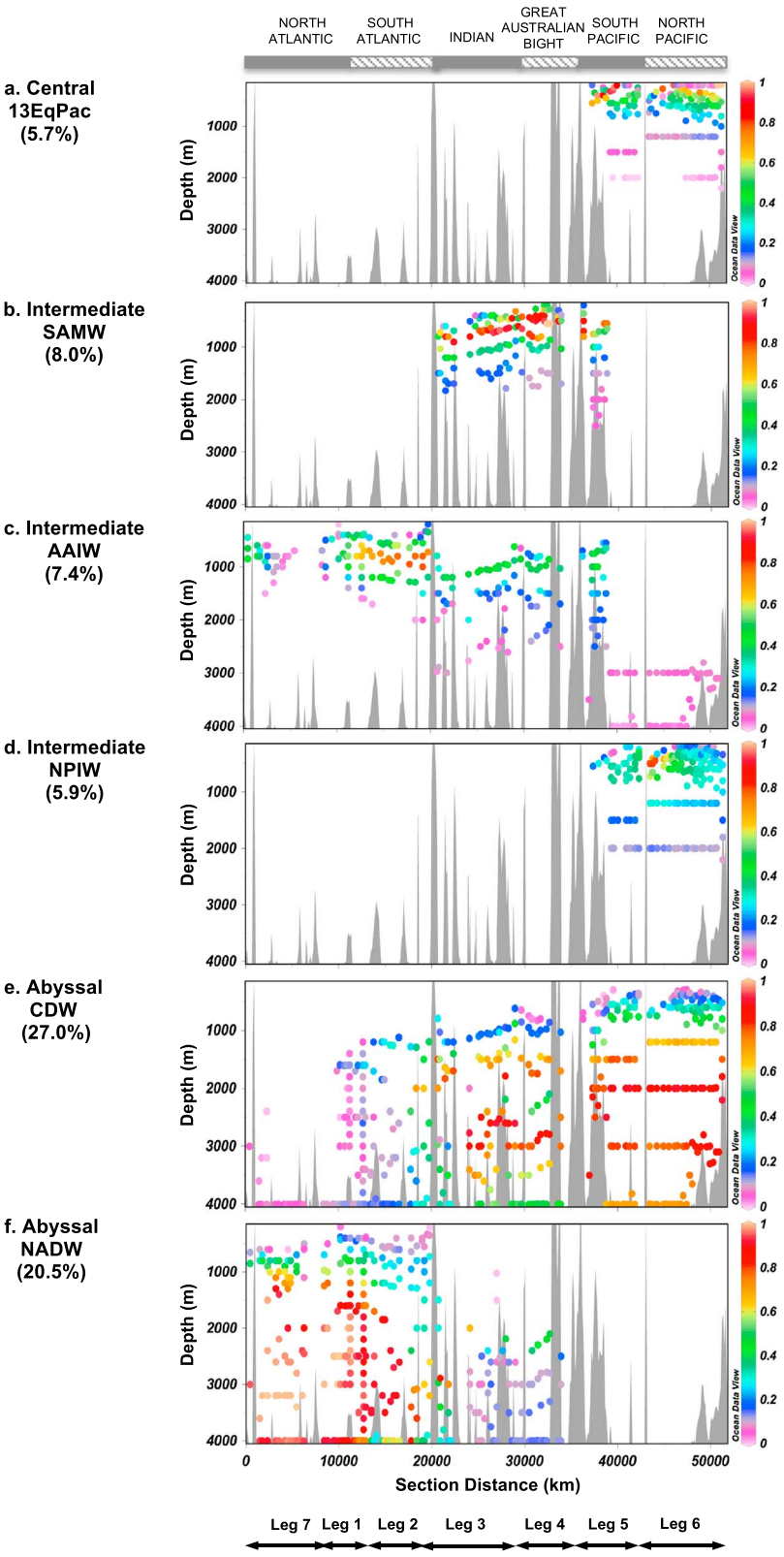

Figure 2. Distribution of the most representative water masses of the dark global ocean during the Malaspina 2010 circumnavigation: (a) Equatorial Pacific Central Water at 13 °C (13EqPac), (b) Sub-Antarctic Mode Water (SAMW), (c) Antarctic Intermediate Water (AAIW), (d) North Pacific Intermediate Water (NPIW), (e) Circumpolar Deep Water (CDW), and (f) North Atlantic Deep Water (NADW). Note that the proportion ranges from 0 (0%) to 1 (100%) and the depth range starts at 200 m.

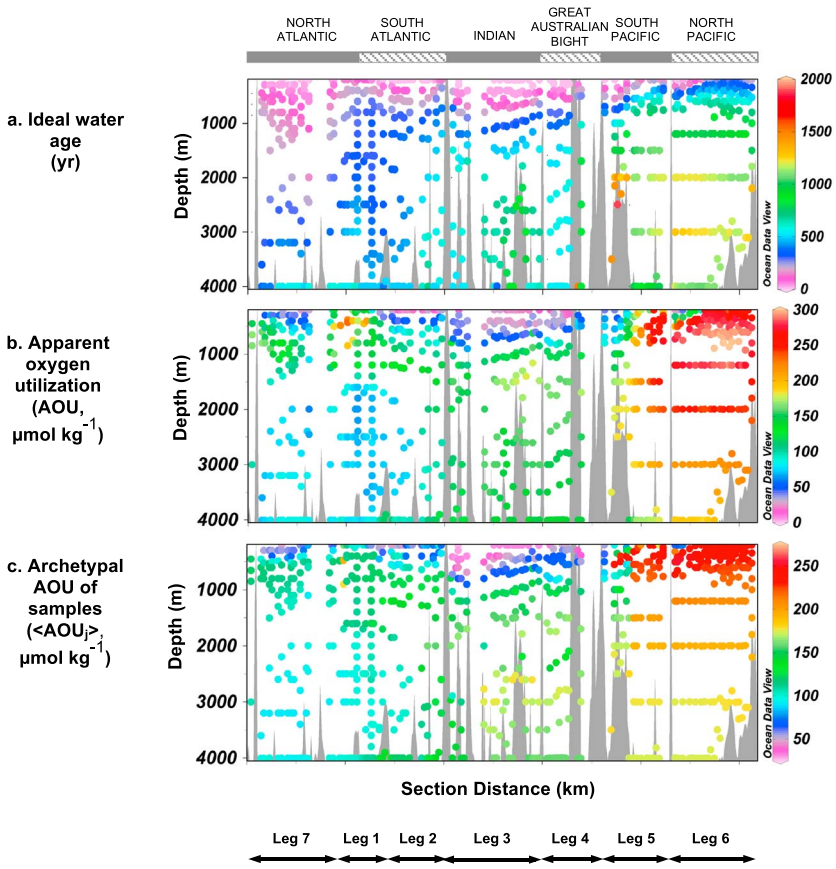

Figure 3. Distribution of (a) ideal water age (τ, years), (b) apparent oxygen utilization (AOU, µmol kg^{-1}), and (c) arquetypal apparent oxygen utilization ($<AOU_j>$, µmol kg^{-1}) of the water samples intercepted during the Malaspina 2010 expedition. Note that the depth range starts at 200 m.

SAMW in the Indian Ocean and the Great Australian Bight, at a Z_i of 1066 ± 80 m (Figure 2c), and NPIW, corresponding to 5.9% of the total volume and located in the North Pacific at a Z_i of 671 ± 65 m (Figure 2d). Finally, we intercepted four abyssal WT that accounted for 52.2% and the CDW was the dominant WT in the deep Indian, South Pacific, and North Pacific basins at a Z_i of 2412 ± 76 m, representing 27.0% of the total volume sampled (Figure 2e). The deep Atlantic waters were dominated by the upper + middle (4.6°C) and lower (2°C) branches of the NADW, representing 20.5% of the total sampled water at Z_i of 1582 ± 99 m and 3780 ± 64 m, respectively (WT weighted-average equals to 2649 ± 78 m) (Figure 2f).

3.2. Basin-Scale Characterization: Ideal Water Age (τ), AOU, and OUR

Water ages (τ) of the samples collected in the dark ocean during the circumnavigation ranged between 0 and 1900 years. The oldest waters were tracked in the southern region of the South Pacific at around 2000 m (Figure 3a). AABW and CDW presented the oldest archetypal ages with 745 ± 47 and 821 ± 22 years, respectively (Table 1). The youngest waters were located in the central domain of all ocean basins except in the North Pacific, with ages of 259 ± 16 and 433 ± 34 years for the CMW_{NP} and 13EqPac, respectively. Note that the young waters of the North Atlantic sank deeper into the water column (Figure 3a). The youngest archetypal ages of all WT were 11 ± 4 years for the EDW formed in the Sargasso Sea and 14 ± 17 years for the $STMW_I$ formed in the subtropical gyre of the Indian Ocean (Table 1). The average age of the central, intermediate, and deep waters intercepted by the cruise track were 170 ± 17, 367 ± 33, and 638 ± 20 years, respectively. Overall, the average age of the waters from 200 to 4000 m was 454 ± 22 years.

Table 1. Archetypal Depth (Z_i, m), Potential Temperature (θ_i,°C), Ideal Water Age (τ_i, yr), Apparent Oxygen Utilization (AOU_i, μmol kg^{-1}), Oxygen Utilization Rate (OUR_i, μmol kg^{-1} yr^{-1}), Absorption Coefficient at 325 nm (a_{325i}, m^{-1}), Slope Between 275 and 295 nm ($S_{275\text{-}295i}$, μm^{-1}), Ratio of the Slope Between 275 and 295 nm Divided by the Slope Between 350 and 400 nm (S_{Ri}, unitless) and the Quantum Yield at 340 nm (Φ_{340i}, %) of the Central, Intermediate, and Abyssal Water Mass Intercepted During the Malaspina 2010 Expedition[a]

Acronym	VOL_i (%)	Z_i (m)	θ_i (°C)	τ_i (year)	AOU_i (μmol kg^{-1})	OUR_i (μmol kg^{-1} yr^{-1})	a_{325i} (m^{-1})	$S_{275\text{-}295i}$ (μm^{-1})	S_{Ri} (unitless)	Φ_{340i} (%)
EDW	0.7	264 ± 20	17.1 ± 0.3	11 ± 4	46 ± 8	4 ± 2	0.26 ± 0.04	28 ± 2	3.4 ± 0.2	0.7 ± 0.1
$ENACW_{12}$	3.2	641 ± 40	10.7 ± 0.4	103 ± 9	114 ± 8	1.1 ± 0.2	0.24 ± 0.02	25 ± 1	2.7 ± 0.1	1.0 ± 0.1
$ENACW_{15}$	1.8	327 ± 25	15.3 ± 0.4	28 ± 7	63 ± 8	2.3 ± 0.9	0.26 ± 0.02	28 ± 1	2.9 ± 0.2	0.8 ± 0.1
13EqAtl	1.6	427 ± 37	11.1 ± 0.8	134 ± 18	61 ± 7	0.5 ± 0.1	0.17 ± 0.02	30 ± 2	2.6 ± 0.2	1.1 ± 0.1
$SACW_{12}$	2.2	303 ± 26	12.2 ± 0.6	104 ± 16	110 ± 16	1.1 ± 0.3	0.20 ± 0.01	26 ± 1	2.6 ± 0.2	1.0 ± 0.1
$SACW_{18}$	1.4	211 ± 11	15.9 ± 0.4	21 ± 9	38 ± 12	2 ± 1	0.18 ± 0.02	31 ± 2	3.2 ± 0.2	0.8 ± 0.1
$STMW_I$	0.9	259 ± 35	14.7 ± 0.4	14 ± 17	26 ± 3	2 ± 2	0.14 ± 0.01	36 ± 2	3.3 ± 0.2	0.9 ± 0.1
ICW_{13}	4.5	395 ± 28	12.2 ± 0.3	51 ± 12	32 ± 2	0.6 ± 0.2	0.15 ± 0.01	33 ± 1	3.1 ± 0.1	0.9 ± 0.1
$STMW_{SP}$	0.2	269 ± 26	13.8 ± 1.5	58 ± 54	49 ± 11	0.9 ± 1.0	0.10 ± 0.03	40 ± 7	3.2 ± 0.3	1.7 ± 0.4
$SPCW_{20}$	0.5	277 ± 84	18.1 ± 21	44 ± 21	70 ± 15	2 ± 1	0.15 ± 0.04	33 ± 4	2.6 ± 0.4	1.1 ± 0.4
13EqPac	5.7	483 ± 35	9.3 ± 0.4	433 ± 34	231 ± 10	0.53 ± 0.07	0.27 ± 0.01	19 ± 1	2.2 ± 0.1	1.0 ± 0.1
CMW_{NP}	3.5	253 ± 13	11.4 ± 0.2	259 ± 16	234 ± 10	0.90 ± 0.09	0.28 ± 0.01	20 ± 1	2.5 ± 0.1	1.0 ± 0.1
$STMW_{NP}$	0.2	207 ± 36	13.7 ± 0.4	141 ± 39	111 ± 6	0.8 ± 0.3	0.21 ± 0.02	26 ± 1	2.7 ± 0.2	1.1 ± 0.1
MW	0.2	1276 ± 354	8.4 ± 1.8	133 ± 42	84 ± 9	0.6 ± 0.3	0.21 ± 0.06	27 ± 5	2.5 ± 0.3	1.3 ± 0.4
SAMW	8.0	719 ± 42	8.1 ± 0.3	214 ± 26	72 ± 6	0.33 ± 0.07	0.16 ± 0.01	29 ± 1	2.6 ± 0.1	1.1 ± 0.1
$AAIW_{5.0}$	2.9	1317 ± 108	4.0 ± 0.2	228 ± 13	128 ± 5	0.56 ± 0.07	0.20 ± 0.02	24 ± 1	2.3 ± 0.1	1.2 ± 0.1
$AAIW_{3.1}$	4.5	677 ± 36	6.9 ± 0.4	499 ± 50	134 ± 5	0.27 ± 0.04	0.18 ± 0.01	23 ± 1	2.1 ± 0.1	1.2 ± 0.1
NPIW	5.9%	671 ± 65	7.3 ± 0.4	571 ± 39	255 ± 6	0.45 ± 0.04	0.28 ± 0.01	18 ± 1	2.1 ± 0.1	1.1 ± 0.1
CDW	27.0%	2412 ± 76	2.5 ± 0.1	821 ± 22	183 ± 4	0.22 ± 0.01	0.21 ± 0.01	19 ± 1	1.8 ± 0.1	1.3 ± 0.1
$NADW_{2.0}$	12.9%	3279 ± 66	2.2 ± 0.1	467 ± 13	88 ± 2	0.19 ± 0.01	0.21 ± 0.01	24 ± 1	2.1 ± 0.1	1.3 ± 0.1
$NADW_{4.6}$	7.6%	1582 ± 99	4.8 ± 0.3	277 ± 13	103 ± 4	0.37 ± 0.03	0.21 ± 0.01	24 ± 1	2.2 ± 0.1	1.3 ± 0.1
AABW	4.7%	3780 ± 64	1.1 ± 0.0	745 ± 47	149 ± 6	0.20 ± 0.02	0.19 ± 0.01	21 ± 1	1.8 ± 0.1	1.5 ± 0.1
R^2 (N_j versus $<N_j>$)					0.80		0.28	0.51	0.42	0.16
SD res					36		0.02	3	0.24	0.2
Determination error					1		0.02	2	0.1	0.12

[a]The percentage of the total volume of water sampled that corresponded to each water mass (VOL_i, %) is also reported. NOTE: EDW: Eighteen Degrees Water, $ENACW_{12}$: Eastern North Atlantic Central Water (12°C), $ENACW_{15}$: Eastern North Atlantic Central Water (15°C), 13EqAtl: equatorial Atlantic Central Water (13°C), $SACW_{12}$: South Atlantic Central Water (12°C), $SACW_{18}$: South Atlantic Central Water (18°C), $STMW_I$: Indian Subtropical Mode Water, ICW_{13}: Indian Central Water (13°C), $STMW_{SP}$: South Pacific Subtropical Mode Water, $SPCW_{20}$: South Pacific Central Water (20°C), 13EqPac: equatorial Pacific Central Water (13°C), CMW_{NP}: North Pacific Central Mode Water (12°C), $STMW_{NP}$: North Pacific Subtropical Mode Water (16°C), MW: Mediterranean Water, SAMW: Sub-Antarctic Mode Water, $AAIW_{3.1}$: Antarctic Intermediate Water (3.1°C), $AAIW_{5.0}$: Antarctic Intermediate Water (5.0°C), NPIW: North Pacific Intermediate Water, $CDW_{1.6}$: Circumpolar Deep Water, $NADW_{2.0}$: North Atlantic Deep Water (2°C), $NADW_{4.6}$: North Atlantic Deep Water (4.6°C), and AABW: Antarctic Bottom Water. The determination error refers to the measurement error for the case of AOU and a_{325}, the propagation of the measurement errors of $F_{(340/360-560)}$ and a_{340} for Φ_{340}, the estimation error of the regression slope for the $S_{275-295}$, and the propagation of the estimation error of the regression slope of $S_{275-295}$ and $S_{350-400}$ for the S_R.

AOU varied between 5 and 299 μmol kg^{-1} (Figure 3b) showing an increase with water mass age along the global overturning circulation (Figure 3a). Maximum AOU_i values were recorded in the central and intermediate waters of the equatorial and North Pacific: NPIW (255 ± 10 μmol kg^{-1}), CMW_{NP} (234 ± 10 μmol kg^{-1}), 13EqPac (231 ± 6 μmol kg^{-1}) (Table 1). Minimum archetypal values corresponded to the central waters of the South Indian and South Atlantic Oceans, with $STMW_I$, ICW_{13}, $SACW_{18}$ presenting 26 ± 2, 32 ± 2 and 38 ± 12 μmol kg^{-1}, respectively (Table 1). The linear regression between the measured (AOU_j) (Figure 3b) and arquetypal ($<AOU_j>$) (Figure 3c) values of AOU in the dark global ocean ($R^2 = 0.80$; Table 1) indicates that 80% of the variability of AOU is retained by the basin-scale mineralization processes from the source region of each water mass to its center of mass in the Malaspina 2010 cruise track.

OUR_i values ranged from 0.2 to 4 μmol kg^{-1} yr^{-1} (Table 1), exhibiting the characteristic power law decrease with depth ($OUR_i = 0.5\ (\pm 0.1)\ (Z_i)^{-0.75(\pm 0.12)}$; $R^2 = 0.67$; $p < 0.05$, Figure S2a in the supporting information). The WT with maximum and minimum OUR_i were the EDW with 4 ± 2 μmol kg^{-1} yr^{-1} and the $NADW_2$ with 0.19 ± 0.01 μmol kg^{-1} yr^{-1}, respectively. The average OUR of the central, intermediate and abyssal waters occupied during the circumnavigation were 1.1 ± 0.4, 0.39 ± 0.06 and 0.23 ± 0.01 μmol kg^{-1} yr^{-1}, respectively, and the average OUR of the waters occupied during the circumnavigation from 200 to 4000 m, hereinafter OUR_{global}, was 0.5 ± 0.1 μmol kg^{-1} yr^{-1}. Extrapolating this rate to the dark global ocean (with a total mass of 1.38×10^{21} kg at a depth > 200 m) yields a total oxygen consumption of 0.68 ± 0.18 Pmol O_2 yr^{-1}.

Most of this oxygen is consumed in the central waters (58%) followed by the abyssal (25%) and, finally, the intermediate (17%) waters.

The dependence of archetypal OUR (OUR_i) on archetypal potential temperature (θ_i) responds to the Arrhenius's law [*Arrhenius*, 1889], exhibiting the expected linear relationship between ln (OUR_i) and the inverse of the absolute potential temperature (Figure S2b in the supporting information):

$$\ln \mathrm{OUR}_i = 46\ (\pm 4) - 108(\pm 10) \cdot \frac{1000}{R \cdot (273.15 + \theta_i)} \qquad \left(R^2 = 0.85,\ n = 22, p < 0.001\right) \tag{13}$$

where R is the gas constant ($8.314\,\mathrm{J\,mol^{-1}\,K^{-1}}$) and $273.15 + \theta_i$ is the absolute archetypal potential temperature. The slope of this relationship, $108 \pm 10\,\mathrm{kJ\,mol^{-1}}$, would represent the activation energy (E_a) of the mineralization of organic matter in the dark global ocean, which translates into a temperature coefficient Q_{10} of 5.2 ± 0.9 as derived with the equation:

$$Q_{10} = e^{\frac{E_a}{R} \cdot \frac{10}{(273.15+\theta_1)\cdot(273.15+\theta_2)}} \tag{14}$$

where θ_1 and θ_2 are the archetypal potential temperatures of the coldest (1.10 ± 0.04°C for AABW) and warmest (18.1 ± 0.8°C for $SPCW_{20}$) WT sampled during the circumnavigation.

3.3. Basin-Scale Characterization: CDOM Quantity and Quality

The values of a_{325} ranged between 0.07 and $0.50\,\mathrm{m^{-1}}$ and changed mostly with section distance, although the a_{325} changes in the Indian Ocean with depth were also relevant (Figure 4a).

The spectral slope $S_{275-295}$ ranged from 8 to $50\,\mu\mathrm{m^{-1}}$, varying with section distance and diminishing with depth. Inversely to the pattern of a_{325}, the highest values were observed at the central and intermediate waters of the South Indian Ocean and the lowest values were located in the intermediate waters of the North Pacific (Figure 4b).

S_R varied between 0.79 and 5.22. It decreased with depth, its maximum values were found in the central waters of the South Indian, and the lowest values were located in the deep waters of Antarctic origin that were less than 1 in some samples (Figure 4c).

Finally, Φ_{340} ranged from 0.3 to 2.9 and increased with depth, presenting maximum values in bottom waters of the South and North Pacific and minimum values in the central waters of the North Atlantic (Figure 4d).

The archetypal values of a_{325}, $S_{275-295}$, S_R, and Φ_{340} in every sample ($<a_{325j}>$, $<S_{275\text{-}295j}>$, $<S_{Rj}>$, and $<\Phi_{340j}>$, respectively) explained 28%, 51%, 42%, and 16% of the total variability of the measured variables (a_{325j}, $S_{275\text{-}295j}$, S_{Rj}, and Φ_{340j}, respectively) in the dark global ocean (Table 1). In the case of a_{325} and Φ_{340}, the fact that the percentages of explained variability were low but significant likely resides in the lack of precision of the CDOM measurements. Note that we have obtained that the standard deviation of the residuals (SD res) of the linear regression between the measured and the arquetypal values of a_{325} and Φ_{340} and the corresponding measurement error of a_{325} and estimation error of Φ_{340} are of the same magnitude (Table 1). Consequently, R^2 were low not because most of the variability of a_{325} and Φ_{340} was not retained by basin-scale changes (or because the unexplained variability at the basin scale was due to variability at the study area) but because of the low sensitivity of the analytical method.

3.4. Dependence of CDOM Variables on Water Mass Aging

Since 80% of the variability of AOU is constrained by basin-scale mineralization processes and water mass mixing, we have used it as tracer of the dynamics of the CDOM variables (Figure 5). In this figure, we show the measured (gray dots) and archetypal values for each sample (black dots) and the archetypal values for each water type (white dots) of a_{325}, $S_{275-295}$, S_R, and Φ_{340}.

The highest a_{325i} values were found in the central and intermediate waters of the North Pacific (NPIW and $CMW_{NP} = 0.28 \pm 0.01\,\mathrm{m^{-1}}$, $13EqPac = 0.27\,\mathrm{m^{-1}} \pm 0.01\,\mathrm{m^{-1}}$) and in a more specific region of the North Atlantic (18–32°N, 17–58°E) ($ENACW_{15} = 0.26 \pm 0.02\,\mathrm{m^{-1}}$, $EDW = 0.26 \pm 0.04\,\mathrm{m^{-1}}$), whereas the lowest a_{325i} were found in the central and intermediate waters of the South Pacific Ocean, with an a_{325i} of $0.10 \pm 0.03\,\mathrm{m^{-1}}$ in the $STMW_{SP}$ (Table 1). The relationship between AOU_i and a_{325i} was positive and significant

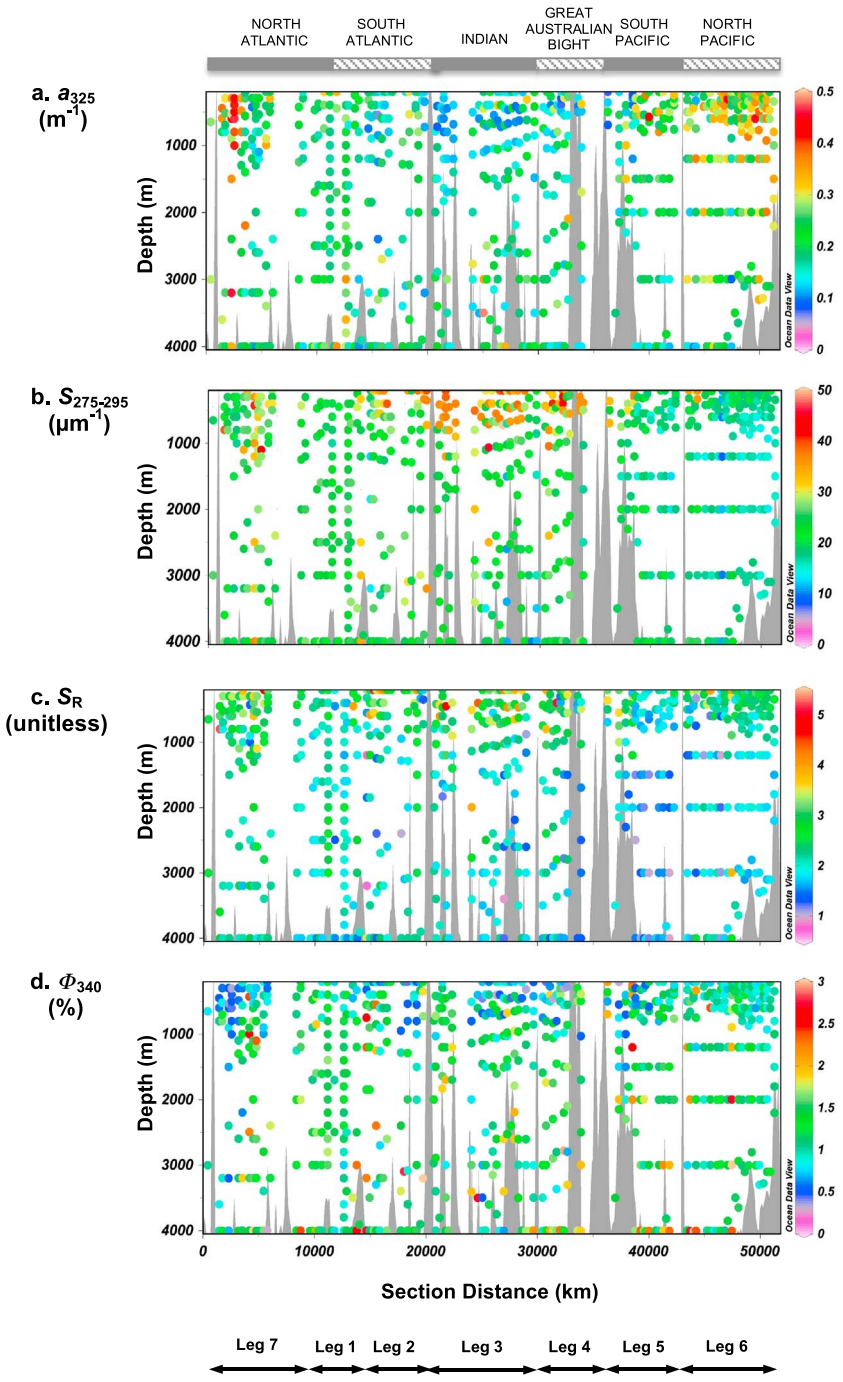

Figure 4. Distribution of (a) a_{325} (m^{-1}), (b) $S_{275-295}$ (μm^{-1}), (c) S_R (unitless), and (d) Φ_{340} (%) of the water samples intercepted during the Malaspina 2010 expedition. Note that the depth range starts at 200 m.

($a_{325i} = 6\,(\pm 1) \times 10^{-4}\,\mathrm{AOU}_i + 0.13\,(\pm 0.01)$, $R^2 = 0.76$, $p < 0.001$, $n = 20$, Figure 5b). Note that ENACW_{15} and EDW were ruled out of the relationship (indigo dots in Figures 5a and 5b). The slope of this relationship ($6 \pm 1 \times 10^{-4}\,\mathrm{m^{-1}\,\mu mol^{-1}\,kg}$) substituted $\frac{\partial a_{325}}{\partial \mathrm{AOU}}$ in equation (10) and was multiplied by the previously obtained $\mathrm{OUR}_{\mathrm{global}}$ of $0.5 \pm 0.1\,\mu\mathrm{mol\,kg^{-1}\,yr^{-1}}$ in equation (11) to obtain a CDOM net production rate NP_{a325} of $3.3 \pm 0.5 \times 10^{-4}\,\mathrm{m^{-1}\,yr^{-1}}$ for the global dark ocean excluding the previously ruled out central waters of the North Atlantic Ocean, which represented only 2.5% of the total volume of sampled water. Following

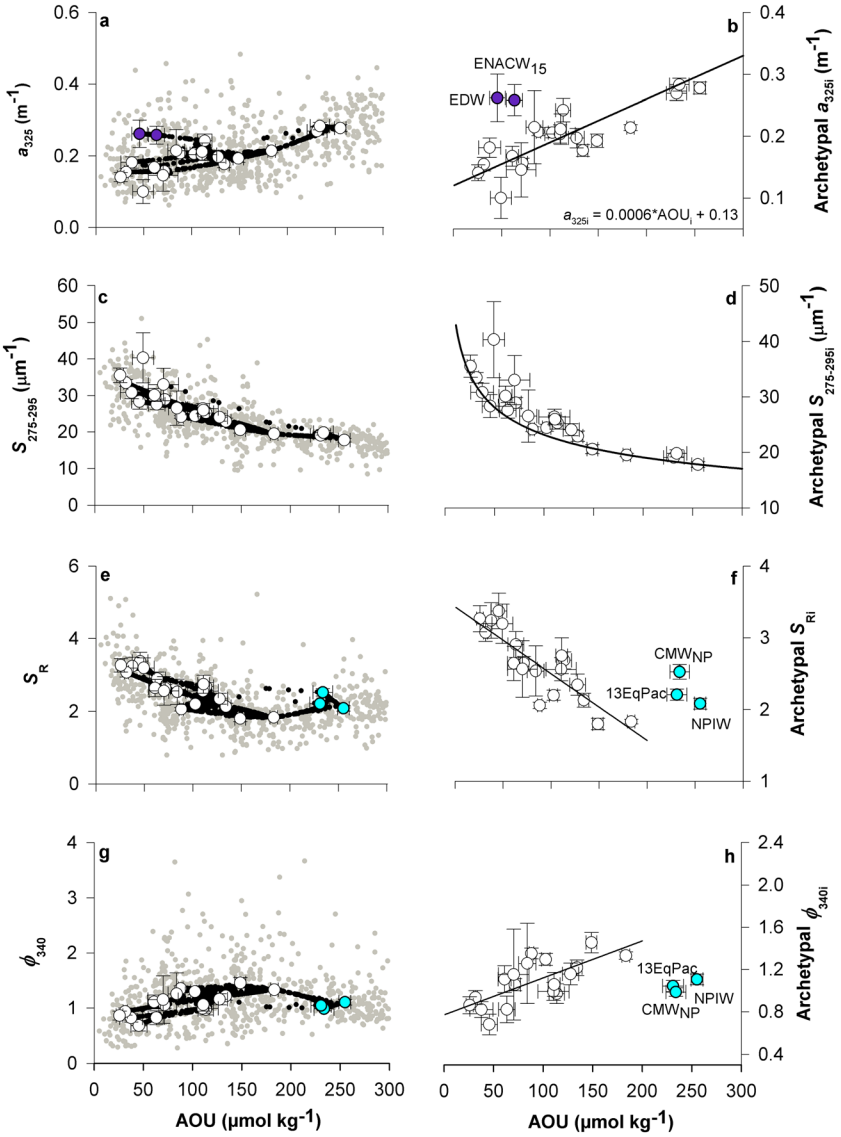

Figure 5. Relationships between the CDOM parameters (a) a_{325}, (m^{-1}), (c) $S_{275–295}$ (μm^{-1}), (e) S_R (unitless), and (g) Φ_{340} (%) with apparent oxygen utilization (AOU, $\mu mol\ kg^{-1}$) in the global dark ocean. In Figures 5a, 5c, 5e, and 5g, measured concentrations (gray dots), archetypal concentrations for each water type (white dots), and archetypal concentrations for each sample (black dots) are presented. Figures 5b, 5d, 5f, and 5h show the relationship between archetypal concentrations of the WT for each studied variable. We obtained the following functions: (b) $a_{325i} = 6\ (\pm 1) \times 10^{-4}\ AOU_i + 0.13\ (\pm 0.01)$, $R^2 = 0.76$ ($p < 0.001$, $n = 20$); (d) $S_{275\text{-}295i} = 0.037\ (\pm 0.002)\ e^{-0.0032(\pm\ 0.0004)\ AOUi}$, $R^2 = 0.82$ ($p < 0.001$, $n = 22$); (f) $S_{Ri} = -0.011\ (\pm 0.002)\ AOU_i + 3.6\ (\pm 0.1)$, $R^2 = 0.74$ ($p < 0.001$, $n = 19$); (h) $\Phi_{340i} = 0.006\ (\pm 0.003)\ AOU_i + 0.60\ (\pm 0.08)$, $R^2 = 0.49$ ($p = 0.001$, $n = 19$). Indigo and sky-blue dots were excluded from their respective regression models (see the text for justification).

equation (12), dividing the WT proportion weighted-average a_{325} of the dark ocean ($0.21 \pm 0.01\ m^{-1}$) by the NP_{a325} calculated above ($3.3 \pm 0.5 \times 10^{-4}\ m^{-1}\ yr^{-1}$), we obtained a CDOM turnover time of 634 ± 120 years.

Contrary to a_{325i}, the qualitative indices $S_{275\text{-}295i}$ and S_{Ri} decreased with water mass aging at an exponential ($S_{275\text{-}295i} = 0.037\ (\pm 0.002)\ e^{-0.0032\ (\pm 0.0004)\ AOU_i}$, $R^2 = 0.82$, $p < 0.001$, $n = 22$, Figure 5d) and linear ($S_{Ri} = -0.011\ (\pm 0.002)\ AOU_i + 3.6\ (\pm 0.1)$, $R^2 = 0.74$, $p < 0.001$, $n = 19$, Figure 5f) rate, respectively. The maximum estimated archetypal values of $S_{275\text{-}295i}$ were 40 ± 7, 36 ± 2 and $33 \pm 1\ \mu m^{-1}$ for the $STMW_{SP}$, $STMW_I$, and ICW_{13}, respectively, and the minimum was $18 \pm 1\ \mu m^{-1}$ for the NPIW (Table 1). The maximum estimated archetypal values of S_{Ri} were 3.4 ± 0.2 for the EDW, 3.3 ± 0.2 for the $STMW_I$ and the minimum S_{Ri} were recorded in the Antarctic WT: AABW and CDW with 1.8 ± 0.1 (Table 1). The Φ_{340i} values increased linearly

with water mass aging ($\Phi_{340i} = 0.006$ (±0.003) $AOU_i + 0.60$ (±0.08), $R^2 = 0.49$, $p = 0.001$, $n = 19$, Figure 5h). Note that the most aged water types (13EqPac, CMW_{NP}, and NPIW; sky blue dots in Figures 5e–5h) were ruled out from both AOU_i-S_{Ri} and AOU_i-Φ_{340i} relationships.

4. Discussion

DOM optical characterization at the global ocean scale can provide insights on the DOC dynamics and the relevance of the microbial carbon pump (MCP) [*Jiao et al*., 2010]. So far, the first attempts to obtain a global inventory of marine CDOM have been focused on the optical characterization of pelagic layers (epipelagic, mesopelagic, and bathypelagic) and ocean basins [*Nelson et al*., 2007, 2010]. The novelty of our work resides in the fact that we have been able to sort the global ocean by water masses (WT), each one showing their intrinsic characteristics of CDOM quantity and quality, and related them with water aging along the global overturning circulation. Our approach, oceanographic rather than geographic, allows to overcome the difficulties encountered by previous attempts (i) several water masses can mix within a given pelagic layer and (ii) the intermediate and abyssal water masses are not usually restricted to a given ocean basin.

It should be noted that *Nelson et al*. [2010] indicated that the average a_{325} of the global ocean at depths between 3000 and 6000 m was $0.14 \pm 0.03\ m^{-1}$ and in the Malaspina circumnavigation the average a_{325} of the 4000 m samples was $0.19 \pm 0.05\ m^{-1}$. It is also relevant to note that the slope of the a_{325}–AOU relationship that we obtained during the circumnavigation ($0.6 \pm 0.1 \times 10^{-4}\ m^{-1}\ \mu mol^{-1}\ kg$) did not differ significantly from the values reported by *Nelson et al*. [2010] for the Indian ($0.62 \times 10^{-3}\ m^{-1}\ \mu mol^{-1}\ kg$) and Pacific ($0.57 \times 10^{-3}\ m^{-1}\ \mu mol^{-1}\ kg$) oceans. Therefore, a constant offset of about $0.05\ m^{-1}$ exists between our a_{325} and those reported by other authors. It is improbable that the fact that we did not filter the samples is the reason behind this dissimilarity (see the detailed description of our procedure in section 2.1.). Note that in the unlikely case that particles represented 10% of the light absorption [*Nelson et al*., 1998], a constant offset of $0.03\ m^{-1}$ would still be present. We surmise that the different methodologies used (double-beam spectrophotometer with linear 10 cm cell versus single-beam spectrophotometer Ultrapath with a 2 m long liquid waveguide capillary cell) may be a feasible cause. An intercalibration between methods would be needed to assess under what conditions both procedures are directly comparable.

4.1. Water Mass Age Versus Aging

Water mass age and aging provide different information; age is defined as the time elapsed since the water was last in contact with the atmosphere, whereas aging (traced through AOU) refers to the consumption of oxygen over that period, which depends on the time elapsed (age) but also on the rate at which dissolved oxygen is consumed during the organic matter mineralization (OUR). Therefore, the AOU variable integrates the OUR over time giving information about how old a water sample is and how fast the mineralization processes occur in that water sample. Although we found a positive and significant power law relationship between AOU and age in the water masses intercepted during the circumnavigation ($AOU_i = 16$ (±5) $\tau_i^{\ 0.34\ (\pm 0.06)}$, $R^2 = 0.72$, $p < 0.001$, $n = 19$, Figure S2c in the supporting information) which explains 72% of their respective global-scale variability, our interest is focused on the 28% of the AOU variability that is not explained by age and is attributed to the quantity and quality of the substrates (particulate, suspended, and dissolved organic matter) that cause a different aging for each WT, i.e., a different OUR_i. Note that CMW_{NP}, 13EqPac, and NPIW were ruled out of the AOU-age correlation because they undergo excessive aging for its age (sky blue dots in Figure S2c in the supporting information).

The average age for the dark global ocean that we obtained (454 ± 22 years) is coherent with previous estimates of 500 years according to *Stuiver et al*. [1983] and 345 years according to *Laruelle et al*. [2009]. It should be noted that *Stuiver et al*. [1983] restricted his estimate to depths > 1500 m. Unlike the Malaspina expedition that only covers a latitude range of 30°N–40°S at depths between 200 and 4000 m, *Laruelle et al*. [2009] estimated the age with a global ocean model considering depths > 200 m. Hence, the absence of central and intermediate waters in the calculation of *Stuiver et al*. [1983] and the consideration of high latitudes (i.e., areas of recent WT formation) in the calculation of *Laruelle et al*. [2009] resulted in a value higher than ours in the case of *Stuiver et al*. [1983] and lower in the case of *Laruelle et al*. [2009].

Our estimate of the dark global ocean oxygen consumption rate (OCR) (0.68 ± 0.18 Pmol O_2 yr^{-1}) is comparable to the 0.83 Pmol O_2 yr^{-1} obtained by *Andersson et al.* [2004] with an ocean biogeochemical model. The difference between these two estimates resides again in the covered domain. The dark global ocean OCR of *Andersson et al.* [2004], which covered the entire ocean, were slightly higher than our estimation (i.e., with a latitude region of 34°N–40°S) because the younger WT of the high latitudes present more elevated OUR which, in turn, raises the dark global ocean OCR. On the contrary, the Malaspina dark global ocean OCR is not comparable with the commonly much higher respiration rates of 2.6–3.5 Pmol O_2 yr^{-1} calculated using in vitro approaches [e.g., *del Giorgio and Duarte*, 2002]. The main reason for this discrepancy is likely that we considered a long timescale that accounts for slower mineralization rates, whereas these authors estimated the mineralization rates at a local and short timescales that reflects mostly the labile carbon.

Our OUR_i values for each WT (0.19–4 μmol O_2 kg^{-1} yr^{-1}) were lower than those found in previous studies [*Álvarez-Salgado et al.*, 2014; *Arístegui et al.*, 2003; *Sarmiento et al.*, 1990; *Jenkins*, 1998]. The higher OUR estimations of 7–16 μmol O_2 kg^{-1} yr^{-1} reported by *Arístegui et al.* [2003] are based on short-term (days) that include mainly the mineralization of labile organic matter. The use of a tracer age equation (applicable to local, short timescale) in *Sarmiento et al.* [1990] and *Jenkins* [1998] also resulted in higher values of 13 μmol O_2 kg^{-1} yr^{-1} and 9 μmol O_2 kg^{-1} yr^{-1}, respectively. In contrast, the use of a tritium box model (applicable to the basin, long timescale) [*Sarmiento et al.*, 1990] led to values of 4–5 μmol O_2 kg^{-1} yr^{-1}, which are closer to our OUR estimations. Furthermore, the high OUR values obtained by *Álvarez-Salgado et al.* [2014], ranging from 6.3 to 18 μmol O_2 kg^{-1} yr^{-1}, are likely associated to their age calculations. Their water age estimate from chlorofluorocarbon (CFC) concentrations tends to underestimate turbulent mixing leading to an underestimation of water mass ages and consequently overestimation of OUR values [*Sonnerup*, 2001; *Mecking et al.*, 2004].

4.2. Recalcitrant Nature of CDOM and Its Origin

The turnover time of 634 ± 120 years that we obtained by combining the NP_{a325} rate ($3.3 \pm 0.5 \times 10^{-4}$ m^{-1} yr^{-1}) and the water mass weighted-average CDOM (0.21 ± 0.01 m^{-1}) gives evidence of the recalcitrant nature of this DOM pool. This turnover time is about 40% longer than the 454 ± 22 years age of the dark global ocean (see section 4.1) and the 435 ± 41 years turnover time of the humic-like fluorescence component 1 (Ex/Em maximum in the UVA/visible at 270–370/470 nm), but not significantly different from the turnover time of the humic-like fluorescence component 2 (Ex/Em maximum in the UVA/visible at 320/400 nm, 610 ± 55 years) recently reported by *Catalá et al.* [2015]. Similarly, the CDOM turnover time, which represents a minimum fraction of the DOC pool, was about 70% longer than the lifetime of the bulk DOC pool (370 years according to *Hansell et al.* [2009]), or the tyrosine-like component 4 (Ex/Em maxima in the UVA/visible at 270/310 nm, 379 ± 98 years according to *Catalá et al.* [2015]), which implies a more recalcitrant nature of the CDOM pool than the bulk DOC pool and, therefore, a larger capability to sequester anthropogenic CO_2.

The E_a and Q_{10} that we obtained for OUR in this study (108 ± 10 kJ mol^{-1} and 5.2 ± 0.9, respectively) were approximately 3 and 2 times higher than the expected values for the labile and the semilabile DOM. *Seiki et al.* [1991] analyzed the temperature dependence of the decomposition of labile phytoplankton-derived organic matter and obtained E_a and Q_{10} values of 37 ± 3 kJ mol^{-1} and < 2, respectively. *Bussmann* [1999] reported E_a and Q_{10} values of 67 ± 11 kJ mol^{-1} and about 3, respectively, for the decomposition of semilabile humic substances. As for the case of the decomposition of soil organic carbon, the association of a higher refractivity to a higher sensitiveness to temperature changes [*Davidson and Janssens*, 2006] and the elevated E_a and Q_{10} of decomposed organic matter in the dark global ocean indicates an enhanced response to temperature which may have implications for the response of the ocean carbon cycle to global warming.

The terrestrial versus the marine origin of this colored recalcitrant fraction of DOM is still controversial. In a study performed in the equatorial Atlantic, *Andrew et al.* [2013] found evidences to support that marine CDOM is composed of a major terrestrial component, founding the increase of CDOM fluorescence with AOU on the charge-transfer model of *Del Vecchio and Blough* [2004], which proposed that the fluorescence signal of DOM is in part due to intramolecular charge-transfer interactions between electron donors and acceptors formed through the partial oxidation of lignin and other aromatic polymeric precursors of terrestrial origin. On the contrary, other studies demonstrated that marine CDOM is generated in situ from

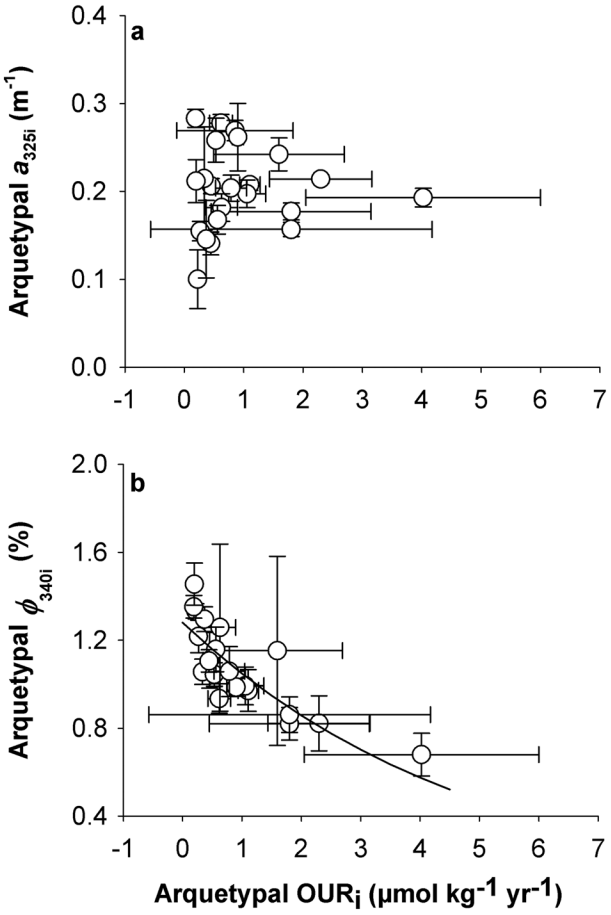

Figure 6. Relationships between archetypal OUR_i (µmol kg^{-1} yr^{-1}) and (a) archetypal a_{325i} (m^{-1}) and (b) archetypal Φ_{340i}. The fitted equation is: $\Phi_{340i} = 1.28\ (\pm 0.05)\ e^{-0.20\ (\pm 0.04)\ OURi}$, $R^2 = 0.55$ ($p = 0.0001$, $n = 22$).

bacterioplankton during its active growth [*Kramer and Herndl*, 2004; *Ortega-Retuerta et al.*, 2009], as well as directly by phytoplankton via extracellular release [*Romera-Castillo et al.*, 2010] or indirectly by zooplankton grazing [*Urban-Rich et al.*, 2006]. Recently, *Jørgensen et al.* [2014] observed an increase in recalcitrant CDOM fluorescence associated with prokaryote utilization of either glucose or natural colorless semilabile DOM as carbon sources. Our positive relationship of a_{325} with AOU (Figures 5a and 5b) is compatible with both hypotheses, which are not mutually exclusive. The terrestrial discharges do not seem to be provoking the elevated initial a_{325i} values of the North Atlantic central water types EDW and $ENACW_{15}$. It should be noted that the low latitudes where these WTs are formed involve warm initial temperatures (θ) of 18°C for the EDW and 15°C for the $ENACW_{15}$ but also elevated photobleaching rates, which should result in relatively high S_{Ri} but low a_{325i} values. In fact, the archetypal S_R values of these WTs are high, 3.4 ± 0.2 for EDW and 2.9 ± 0.2 for $ENACW_{15}$; however, the archetypal values of a_{325} are relatively high and favor us to propose that, prior to winter mixing, enhanced microbial production of CDOM in these warm water masses exceeded removal by photobleaching leading to high initial a_{325} and S_R during their formation. The high a_{325} values of the central North Atlantic are of the same level than those found in the thermocline waters of the North Pacific, specifically CMW_{NP}, 13EqPac, and NPIW (Table 1 and Figures 4a, 5a, and 5b). However, in this case, they are not due to high initial a_{325} values but to the excessive aging experienced by these WT for its age, which is associated with (i) the sluggish circulation of the North Pacific that allows recalcitrant CDOM accumulation, (ii) the large size of the North Pacific subtropical gyre, resulting in large distances from the edge to the center of the gyre, where downwelling occurs, and (iii) the export of particulate organic material that results in high oxygen utilization rates [*Feely et al.*, 2004] and production of recalcitrant CDOM [e.g., *Hayase and Shinozuka*, 1995; *Yamashita et al.*, 2007; *Yamashita and Tanoue*, 2008, 2009].

4.3. Factors Controlling the CDOM Quantity and Quality in the Global Ocean

Not only the magnitude (AOU) but also the rate of mineralization (OUR) are key variables to understand the basin-scale variability of the quantity and quality of CDOM. In general terms, an old water mass presents slow mineralization rates caused by either an insufficient (limiting) or biologically recalcitrant substrate, leading to low OUR [*Jenkins*, 1998].

To check the variable—aging (AOU) or substrate quantity and quality (OUR)—that better contributes to explain the variability of CDOM in the dark global ocean, we performed two simple regression analyses, one considering the AOU_i and another considering OUR_i as independent variables. The a_{325i} values represent quantity, and Φ_{340}, which is an appropriate (but still not broadly used) proxy to CDOM aromaticity, was taken as a qualitative variable (Figure 6). For the case of a_{325i}, the regression analysis was positive and significant with AOU_i, explaining 76% of the variability of a_{325i} ($R^2 = 0.76$, Figure 5b), but was not significant with OUR_i (Figure 6a). This means that aging is the key variable to explain the accumulation

of CDOM in the dark global ocean (i.e., for a same age, the WT that has experienced faster mineralization rates will have more CDOM). Conversely, for the case of Φ_{340i}, it is not AOU_i (Figure 5h) but OUR_i (Figure 6b) the variable that best explains its variability, with the following inverse relationship, $\Phi_{340i} = 1.28\ (\pm 0.05)\ e^{-0.20\ (\pm 0.04)\ OURi}$ ($R^2 = 0.55$, $p = 0.001$, $n = 22$). This means that the lower the rate of mineralization, the higher the aromaticity of the CDOM generated by microbial respiration. Therefore, the lower the quality for microbial consumption of the mineralized organic matter, the more complex the DOM molecular structures and the more content in aromatic compounds, promoting the ability to emit fluorescence. This assumption matches with the novel results of *Jørgensen et al*. [2014] that confirms that the more recalcitrant the mineralized materials the larger the production rate of fluorescent DOM. It can also be coherent with the charge-transfer model of *Del Vecchio and Blough* [2004] regarding the terrestrial origin of CDOM in the ocean that were previously mentioned in section 4.2.

Linked to the same postulation, we found that the lowest $S_{275\text{-}295i}$ and S_{Ri} values corresponded to the oldest WT (Figures 5d and 5f), and, according to *Helms et al*. [2008], low values are attributed to a dominant content of aromatic and high molecular weight (HWM) DOM fraction. However, this hypothesis, indicating that the low molecular weight (LMW) DOM turns into to a more recalcitrant HMW DOM with aging, does not appear to apply to the bulk of natural DOM according to *Amon and Benner* [1996]. Instead, they found that the bulk of HMW DOM is more bioreactive and fresher than the LMW DOM. Consequently, it seems that both synthesis and transformation of the HMW RDOM happen during the DOM mineralization.

Our study is the first in presenting a global data set of S_R for the entire dark ocean, allowing to differentiate the S_R of the various WT within the ocean rather than just contrasting the wide difference between terrestrial and marine sources of CDOM in coastal areas. Similar to *Helms et al*. [2008], we obtained a linear and positive relationship between salinity (S) and S_R but within the much narrower salinity range of the open ocean waters ($S_{Ri} = 0.85\ (\pm 0.22)\ (S_i) - 27\ (\pm 8)$, $R^2 = 0.43$, $p = 0.001$, $n = 22$, Figure S2d in the supporting information). However, whereas in the case of *Helms et al*. [2008] the relationship is related to the terrestrial versus marine origin of the samples, in the case of our open ocean samples, it is presumably produced by photobleaching. The positive relationship can be justified because saltier water masses are generally originated at lower latitudes where photobleaching previous to winter convection is higher. In order to check this, we have used the potential temperature (θ) as a proxy to the exposure of the water masses to solar radiation and, therefore, we have related S_R with θ. It resulted that the linear regression with θ ($S_{Ri} = 0.09\ (\pm 0.01)\ (\theta_i) + 1.77\ (\pm 0.12)$, $R^2 = 0.74$, $p = 0.001$, $n = 22$) explained the global distribution of S_R better than S. Note that higher θ results in higher S_R values and lower molecular weight of CDOM (i.e., lower content in aromatic substances). This means that the relationship between S_R and S may also express the degree of photobleaching when considering the open ocean.

5. Conclusions

This study provides (1) the first global inventory of CDOM variables of the main water masses of the ocean; (2) a robust estimate of the turnover time of CDOM in the dark global ocean of 634 ± 120 years, which exceeds the turnover time of the DOC pool and the water flushing time of the dark ocean by 70% and 40%, respectively; and (3) new evidences on the dependence of CDOM quantity on water mass aging (AOU) and CDOM quality on the nature of the mineralized organic matter (OUR).

Acknowledgments

We thank C.M. Duarte for the coordination of the Malaspina expedition; the chief scientists of the seven legs, the staff of the Marine Technology Unit (CSIC-UTM) and the Captain and crew of R/V *Hespérides* for their outright support during the circumnavigation. This study was financed by the Malaspina 2010 circumnavigation expedition (grant CSD2008–00077); T.S.C acknowledges funding through a predoctoral fellowship (reference AP2009-2138) from the Ministerio de Educación, Cultura y Deporte. C.R-C. acknowledges funding through a Beatriu de Pinos postdoctoral fellowship from the Generalitat de Catalunya. M.N.-C. was funded by the CSIC Program "Junta para la Ampliación de Estudios" cofinanced by the ESF. S.K. was supported by U.S. NSF grant OCE-1060804. E.F.G. was funded through a JAE-Pre grant from CSIC and the European Social Fund. C. M. was supported by DOREMI (CTM2012-34294) funded by the Spanish Ministry of Economy and Competitiveness.

References

Álvarez-Salgado, X. A., M. Nieto-Cid, M. Álvarez, F. F. Pérez, P. Morin, and H. Mercier (2013), New insights on the mineralization of dissolved organic matter in central, intermediate, and deep water masses of the northeast North Atlantic, *Limnol. Oceanogr.*, *58*, 681–696.

Álvarez-Salgado, X. A., M. Álvarez, S. Brea, L. Mèmery, and M. J. Messias (2014), Mineralization of biogenic materials in the water masses of the South Atlantic Ocean. II: Stoichiometric ratios and mineralization rates, *Prog. Oceanogr.*, *123*, 24–37.

Amon, R. M. W., and R. Benner (1996), Bacterial utilization of different size classes of disolved organic matter, *Limnol. Oceanogr.*, *41*(1), 41–51.

Andersson, J. H., J. W. M. Wijsman, P. M. J. Herman, J. J. Middelburg, K. Soetaert, and C. Heip (2004), Respiration patterns in the deep ocean, *Geophys. Res. Lett.*, *31*, L03304, doi:10.1029/2003GL018756.

Andrew, A. A., R. Del Vecchio, A. Subramaniam, and N. V. Blough (2013), Chromophoric dissolved organic matter (CDOM) in the equatorial Atlantic Ocean: Optical properties and their relation to CDOM structure and source, *Mar. Chem.*, *148*, 33–43, doi:10.1016/j.marchem.2012.11.001.

Arístegui, J. S., S. Agustí, and C. M. Duarte (2003), Respiration in the dark ocean, *Geophys. Res. Lett.*, *30*(2), 1041, doi:10.1029/2002GL016227.

Arrhenius, S. Z. (1889), Über die reaktionsgeschwindigkeit bei der inversion von rohrzucker durch säuren, *Phys. Chem.*, *4*, 226–248.

Arrieta, J. M., E. Mayol, R. L. Hansman, G. J. Herndl, T. Dittmar, and C. M. Duarte (2015), Dilution limits dissolved organic carbon utilization in the deep ocean, *Science*, *348*(6232), 331–333, doi:10.1126/science.1258955.

Benner, R., and G. Herndl (2011), Bacterially derived dissolved organic matter in the microbial carbon pump, in *Microbial Carbon Pump in the Ocean*, edited by N. Jiao, F. Azam, and S. Sanders, pp. 46–48, Science/AAAS, Washington, D. C., doi:10.1126/science.opms.sb0001.
Benson, B. B., and D. Krauss Jr. (1984), The concentration and isotopic fractionation of oxygen dissolved in freshwater and seawater in equilibrium with the atmosphere, *Limnol. Oceanogr.*, *29*, 620–632.
Bricaud, A., A. Morel, and L. Prieur (1981), Absorption by dissolved organic matter of the sea (yellow substance) in the UV and visible domains, *Limnol. Oceanogr.*, *26*(l), 43–53.
Brown, M. (1977), Transmission spectroscopy examinations of natural waters, *Estuarine Coastal Mar. Sci.*, *5*, 309–317.
Bussmann, I. (1999), Bacterial utilization of humic substances from the Arctic Ocean, *Aquat. Microb. Ecol.*, *19*, 37–45.
Carlson, C. A., H. W. Ducklow, and A. F. Michaels (1994), Annual flux of dissolved organic carbon from the euphotic zone in the northwestern Sargasso Sea, *Nature*, *371*, 405–408.
Catalá, T. S., et al. (2015), Turnover time of fluorescent dissolved organic matter in the dark global ocean, *Nat. Commun.*, *6*, 5986, doi:10.1038/ncomms6986.
Davidson, E. A., and I. Janssens (2006), Temperature sensitivity of soil carbon decomposition and feedbacks to climate change, *Nature*, *440*, 165–173.
del Giorgio, P., and C. M. Duarte (2002), Respiration in the open ocean, *Nature*, *420*, 379–384.
Del Vecchio, R., and N. V. Blough (2004), On the origin of the optical properties of humic substances, *Environ. Sci. Technol.*, *38*, 3885–3891.
Feely, R. A., C. L. Sabinelli, R. Schlitzer, J. L. Bullister, S. Mecking, and D. Greeley (2004), Remineralization in the upper water column of the Pacific Ocean, *J. Oceanogr.*, *60*, 45–52.
Green, S. A., and N. V. Blough (1994), Optical absorption and fluorescence properties of chromophoric dissolved organic matter in natural waters, *Limnol. Oceanogr.*, *39*, 1903–1916.
Gruber, N., et al. (2009), Oceanic sources, sinks, and transport of atmospheric CO_2, *Global Biogeochem. Cycles*, *23*, GB1005, doi:10.1029/2008GB003349.
Hansell, D. A. (2013), Recalcitrant dissolved organic carbon fractions, *Annu. Rev. Mar. Sci.*, *5*, 421–425, doi:10.1146/annurev-marine-120710-100757.
Hansell, D. A., C. A. Carlson, D. J. Repeta, and S. Reiner (2009), Dissolved organic matter in the ocean: New insights stimulated by a controversy, *Oceanography*, *22*, 52–61.
Hansell, D. A., C. A. Carlson, and R. Schlitzer (2012), Net removal of major marine dissolved organic carbon fractions in the subsurface ocean, *Global Biogeochem. Cycles*, *26*, GB1016, doi:10.1029/2011GB004069.
Hayase, K., and N. Shinozuka (1995), Vertical distribution of fluorescent organic matter along with AOU and nutrients in the equatorial Central Pacific, *Mar. Chem.*, *48*, 283–290.
Hedges, J. I. (1992), Global biogeochemical cycles: Progress and problems, *Mar. Chem.*, *39*, 67–93.
Helms, J. R., A. Stubbins, J. D. Ritchie, E. C. Minor, D. J. Kieber, and K. Mopper (2008), Absorption spectral slopes and slope ratios as indicators of molecular weight, source, and photobleaching of chromophoric dissolved organic matter, *Limnol. Oceanogr.*, *53*, 955–969.
Helms, J. R., A. Stubbins, E. M. Perdue, N. W. Green, H. Chen, and K. Mopper (2013), Photochemical bleaching of oceanic dissolved organic matter and its effect on absorption spectral slope and fluorescence, *Mar. Chem.*, *155*, 81–91.
Ito, T., M. J. Follows, and E. A. Boyle (2004), Is AOU a good measure of respiration in the oceans?, *Geophys. Res. Lett.*, *31*, L17305, doi:10.1029/2004GL020900.
Jenkins, W. J. (1982), Oxygen utilization rates in the North Atlantic subtropical gyre and primary production in oligotrophic systems, *Nature*, *300*, 246–249.
Jenkins, W. J. (1998), Studying subtropical thermocline ventilation and circulation using tritium and ^{3}He, *J. Geophys. Res.*, *103*, 15,817–15,831, doi:10.1029/98JC00141.
Jiao, N., et al. (2010), Microbial production of recalcitrant dissolved organic matter: Long-term carbon storage in the global ocean, *Nat. Rev. Microbiol.*, *8*, 593–599.
Jørgensen, L., C. A. Stedmon, M. A. Granskog, and M. Middelboe (2014), Tracing the long-term microbial production of recalcitrant fluorescent dissolved organic matter in seawater, *Geophys. Res. Lett.*, *41*, 2481–2488, doi:10.1002/2014GL059428.
Karstensen, J., and M. Tomczak (1998), Age determination of mixed water masses using CFC and oxygen data, *J. Geophys. Res.*, *103*(C9), 18,599–18,609, doi:10.1029/98JC00889.
Kattner, G., M. Simon, and B. P. Koch (2011), Molecular characterization of dissolved organic matter and constraints for prokaryotic utilization, in *Microbial Carbon Pump in the Ocean*, edited by N. Jiao, F. Azam, and S. Sanders, pp. 60–61, Science/AAAS, Washington, D. C., doi:10.1126/science.opms.sb0001.
Khatiwala, S., F. Primeau, and T. Hall (2009), Reconstruction of the history of anthropogenic CO_2 concentrations in the ocean, *Nature*, *462*, 346–349, doi:10.1038/nature08526.
Khatiwala, S., F. Primeau, and M. Holzer (2012), Ventilation of the deep ocean constrained with tracer observations and implications for radiocarbon estimates of ideal mean age, *Earth Planet. Sci. Lett.*, *325–326*, 116–125.
Kramer, G. D., and G. L. Herndl (2004), Photo- and bioreactivity of chromophoric dissolved organic matter produced by marine bacterioplankton, *Aquat. Microb. Ecol.*, *36*, 239–246.
Laruelle, G. G., et al. (2009), Anthropogenic perturbations of the silicon cycle at the global scale: Key role of the land-ocean transition, *Global Biogeochem. Cycles*, *23*, GB4031, doi:10.1029/2008GB003267.
Mecking, S., M. J. Warner, C. E. Greene, S. L. Hautala, and R. E. Sonnerup (2004), Influence of mixing on CFC uptake and CFC ages in the North Pacific thermocline, *J. Geophys. Res.*, *109*, C07014, doi:10.1029/2003JC001988.
Melhuish, W. H. (1961), Quantum efficiencies of fluorescence of organic substances: Effect of solvent and concentration of the fluorescent solute, *J. Phys. Chem.*, *65*, 229–235.
Nelson, N. B., and D. A. Siegel (2013), The global distribution and dynamics of chromophoric dissolved organic matter, *Annu. Rev. Mar. Sci.*, *5*, 447–476.
Nelson, N. B., D. A. Siegel, and A. F. Michaels (1998), Seasonal dynamics of colored disolved material in the Sargasso Sea, *Deep Sea Res., Part I*, *45*, 931–957.
Nelson, N. B., D. A. Siegel, C. A. Carlson, C. M. Swan, W. M. Smethie, and S. Khatiwala (2007), Hydrography of chromophoric dissolved organic matter in the North Atlantic, *Deep Sea Res., Part I*, *54*, 710–731.
Nelson, N. B., D. A. Siegel, C. A. Carlson, and C. M. Swan (2010), Tracing global biogeochemical cycles and meridional overturning circulation using chromophoric dissolved organic matter, *Geophys. Res. Let.*, *37*, L03610, doi:10.1029/2009GL042325.
Ogawa, H., Y. Amagai, I. Koike, K. Kaiser, and R. Benner (2001), Production of refractory dissolved organic matter by bacteria, *Science*, *292*, 917–20.
Ortega-Retuerta, E., T. K. Frazer, C. M. Duarte, S. Ruiz-Halpern, A. Tovar-Sanchez, J. M. Arrieta, and I. Reche (2009), Biogeneration of chromophoric dissolved organic matter by bacteria and krill in the Southern Ocean, *Limnol. Oceanogr.*, *54*(6), 1941–1950.

Ortega-Retuerta, E., D. A. Siegel, N. B. Nelson, C. M. Duarte, and I. Reche (2010), Observations of chromophoric dissolved and detrital organic matter distribution using remote sensing in the Southern Ocean: Validation, dynamics and regulation, *J. Mar. Syst.*, *82*, 295–303.
Romera-Castillo, C., H. Sarmento, X. A. Álvarez-Salgado, J. M. Gasol, and C. Marrasé (2010), Production of chromophoric dissolved organic matter by marine phytoplankton, *Limnol. Oceanogr.*, *55*(1), 446–454.
Romera-Castillo, C., M. Nieto-Cid, C. G. Castro, C. Marrasé, J. Largier, E. D. Barton, and X. A. Álvarez-Salgado (2011), Fluorescence: Absorption coefficient ratio—Tracing photochemical and microbial degradation processes affecting coloured dissolved organic matter in a coastal system, *Mar. Chem.*, *125*, 26–38.
Sarmiento, J., G. Thiele, R. Key, and W. Moore (1990), Oxygen and nitrate new production and remineralization in the North Atlantic subtropical gyre, *J. Geophys. Res.*, *95*(C10), 18,303–18,315, doi:10.1029/90JC01049.
Seiki, T., E. Date, and H. Izawa (1991), Decomposition characteristics of particulate organic matter in Hiroshima Bay, *J. Oceangr.*, *47*, 207–220.
Siegel, D. A., S. Maritorena, N. B. Nelson, M. J. Behrenfeld, and C. R. McClain (2005), Colored dissolved organic matter and its influence on the satellite-based characterization of the ocean biosphere, *Geophys. Res. Lett.*, *32*, L20605, doi:10.1029/2005GL024310.
Siegenthaler, U., and J. L. Sarmiento (1993), Atmospheric carbon dioxide and the ocean, *Nature*, *365*, 119–125.
Six, K. D., and E. Maier-Reimer (1996), Effects of plankton dynamics on seasonal carbon fluxes in an ocean general circulation model, *Global Biogeochem. Cycles*, *10*, 559–583, doi:10.1029/96GB02561.
Sokal, F. F., and F. J. Rohlf (1995), *Biometry: The Principles and Practice of Statistics in Biological Research*, 3rd ed., 937 pp., W. H. Freeman and Co., New York.
Sonnerup, R. E. (2001), On the relations among CFC derived water mass ages, *Geophys. Res. Lett.*, *28*(9), 1739–1742, doi:10.1029/2000GL012569.
Stuiver, M., P. D. Quay, and H. G. Ostlund (1983), Abyssal water carbon-14 distribution and the age of the world oceans, *Science*, *219*(4586), 849–851.
Tomczak, M. (1999), Some historical, theoretical and applied aspects of quantitative water mass analysis, *J. Mar. Res.*, *57*, 275–303.
Twardowski, M. S., E. Boss, J. M. Sullivan, and P. L. Donaghay (2004), Modeling the spectral shape of absorbing chromophoric dissolved organic matter, *Mar. Chem.*, *89*, 69–88.
Urban-Rich, J., D. Fernández, and J. L. Acuña (2006), Grazing impact on chromophoric dissolved organic matter (CDOM) by the larvacean Oikopleura dioica, *Mar. Ecol. Prog. Ser.*, *317*, 101–110.
Weishaar, J. L., G. R. Aiken, B. A. Bergamaschi, M. S. Fram, R. Fugii, and K. Mopper (2003), Evaluation of specific ultraviolet absorbance as an indicator of the chemical composition and reactivity of dissolved organic carbon, *Environ. Sci. Technol.*, *37*, 4702–4708.
Yamashita, Y., and E. Tanoue (2008), Production of bio-refractory fluorescent disolved organic matter in the ocean interior, *Nature, 1*, 579–582.
Yamashita, Y., and E. Tanoue (2009), Basin scale distribution of chromophoric dissolved organic matter in the Pacific Ocean, *Limnol. Oceanogr.*, *54*, 598–609.
Yamashita, Y., A. Tsukasaki, T. Nishida, and E. Tanoue (2007), Vertical and horizontal distribution of fluorescent dissolved organic matter in the Southern Ocean, *Mar. Chem.*, *106*, 498–509.